Supplemental Figure Legends

Figure S1. The neutralization activity of DH1047, ADG-2, and REGN 10933 against sarbecoviruses. Neutralization is shown for SARS-CoV-2 B.1.351, SARS-CoV urbani, and RsSHC014. Data are representative of two technical replicates.

Figure S2. The binding activity of cross-reactive antibodies against MERS-CoV and human common-cold coronaviruses. The binding activity of four broadly neutralizing antibodies against SARS-CoV-2 NTD, MERS-CoV spike protein, HCoV-OC43 spike protein, HCoV-NL63 spike protein, and HCoV-229E spike protein is shown for DH1235, DH1073, DH1046, and DH1047. Data are representative of two technical replicates. OD, optical density.

Figure S3. Coronavirus cross-reactive antibodies exhibit distinct binding modes to SARS-CoV-2 receptor binding domain (RBD). (**A**) Three-dimensional reconstruction from negative stain electron microscopic images of DH1073 (purple) in complex with Hexapro stabilized SARS-CoV-2 Spike ectodomain (gray). On the left and center, the map is shown in two orthogonal views. On the right, the map is shown as a transparent surface, rigidly fit with a 1-RBD-up spike model, PDB ID: 6ACK. (**B**) Three-dimensional reconstruction of DH1235 (blue) in complex with Hexapro stabilized Spike ectodomain (gray). The rigidly fit 3-RBD-up spike model on the right was generated from PDB ID: 6ACK. Fit models in (A) and (B) were used to compare the binding of DH1073 and DH1235 to known RBD-directed nAbs. (**C**) Four orthogonal views of RBD binding by DH1073 (purple) and DH1235 (blue), compared to known RBD nAbs, shown as molecular surface: C105 (pale cyan, Class 1, PDG ID 6XCN and 6XCA),

DH1041 (light blue, Class 2, PDB ID: 7LAA), S309 (wheat, Class 3, PDB ID: 7BEP), CR3022 (pink, Class 4, PDB ID: 6W41), and DH1047 (green, PDB ID: 7LD1). The last two views correspond to the same views shown in Fig. 3D. DH1073 overlaps with DH1235, C105 (Class 1) and CR3022 (Class 4). DH1235 overlaps DH1073, DH1047, C105 and CR3022. (**D**) Antibody competition for binding to SARS-CoV-2 spike protein stabilized with two prolines (S-2P) is shown by results from surface plasmon resonance (SPR) assays. The antibody used to capture S-2P is shown as the row title. The antibody flowed over the captured spike is shown as column titles. + indicates blocking and competition; - indicates no blocking of binding and no competition.

Figure S4. Negative Stain Electron Microscopy (NSEM) of DH1047 bound to bat RsSHC014 and SARS-CoV spike ectodomains. (**A**) Representative 2D class averages of bat RsSHC014 S-2P ectodomain bound to DH1047 Fab are shown. (**B**) An overlay of 3D reconstructions of DH1047 bound to bat RsSHC014 2P (gray) and SARS-CoV-2 HexaPro (purple) spike ectodomains is shown. (**C**) Representative 2D class averages of SARS-CoV S-2P ectodomain bound to DH1047 Fab are shown. (**D**) An overlay of 3D reconstruction of DH1047 bound to bat SARS-CoV 2P (gray) and SARS-CoV-2 HexaPro (purple) spike ectodomains is shown. The red boxes in (A) and (C) indicate the classes that show DH1047 Fab bound to spike.

Figure S5. Cryo-EM data processing for the SARS-CoV spike ectodomain bound to DH1047. (**A**) A representative cryo-EM micrograph is shown. (**B**) Cryo-EM contrast transfer function (CTF) fit is shown. (**C**) Representative 2D class averages from Cryo-EM dataset are shown. (**D and E**) Ab initio reconstruction (D) and a refined map (E) are shown. (**F**) Fourier

shell correlation curves are shown. (**G**) A refined cryo-EM map colored by local resolution is shown. (**H**) Zoom-in images show the SD1, NTD, HR1/CH and RBD/Fab contact regions in the structure. The cryo-EM map is shown as a blue mesh and the fitted model is in cartoon representation, with residues shown as sticks.

Figure S6. The affinity data of DH1047 against SARS-CoV and RsSHC014 spikes. SPR binding experiments of DH1047 against SARS-CoV-2 Toronto and RsSHC014. Binding affinity measurements are shown in the tables and response units (RU) as a function of time in seconds (s) is shown for both SARS-CoV and RsSHC014. SPR experiments were repeated twice.

Figure S7. Hematoxylin and eosin staining of lungs from SARS-CoV infected mice collected at 4 days post infection.

(**A** to **D**) mice were treated with control CH65 antibody prophylactically (**A**) or therapeutically (**B**) or treated with DH1047 antibody prophylactically (**C**) or therapeutically (**D**). Prophylactic treatment was administered 12 hours before infection, and therapeutic treatment was administered 12 hours after infection. Pathologic features of acute lung injury were scored using two separate tools: the American Thoracic Society Lung Injury Scoring (ATS ALI) system. Using this ATS ALI system, we created an aggregate score for the following features: neutrophils in the alveolar and interstitial space, hyaline membranes, proteinaceous debris filling the air spaces, and alveolar septal thickening. Three randomly chosen high power (×60) fields of diseased lung were assessed per mouse. Representative images are shown. All images were taken at the same magnification. The black bar indicates 100 μm scale.

Figure S8. Comparison of DH1047 binding footprint to that of other RBD-directed Abs that bind overlapping epitopes.

(**A**) RBD is shown in black and ACE2 binding footprint is colored yellow. Binding footprints of antibodies DH1047 (PDB: 7LD1), CR3022 (PDB: 6YLA), EY6A (PDB: 6ZCZ), H014 (PDB: 7CAH), COVA1-16 (PDB: 7JMW) and S304 (PDB: 7JW0) are shown in green. (**B)** The overlay shows DH1047 bound RBD and RBD bound to nanobodies VHH V (PDB: 7KN6), VHH W (PDB: 7KN7) and VHH-72 (PDB: 6WAQ).

Figure S9. Binding of DH1047 mutants to the SARS-CoV-2 S-2P ectodomain.

(**A**) Binding assays were performed by Biolayer Interferometry using alanine scanning mutants of DH1047. (Top) Inferometry curves are shown. (Bottom) Binding of DH1047 IgG and mutants to SARS-CoV-2 S-2P ectodomain was normalized to the binding observed for DH1047 WT IgG (dotted line). (**B**) Binding of purified DH1047 WT IgG and selected mutants to SARS-CoV-2 S-2P ectodomain was measured by SPR. The spike was captured by its C-terminal TwinStreptactin tag on a SA chip. Binding to the antibodies was measured by flowing over 200 nM solutions of the IgG in HBS-EP+ buffer. (**C**) The binding interface of DH1047 to RBD (gray) is shown. The DH1047 residues that were mutated are shown as sticks and labeled.

Figure S10. DH1047 and ADG-2 bind the RBD of SARS-CoV and SARS-CoV-2 spike ectodomains using a similar footprint.

(**A**) A cartoon representation is shown for DH1047 (colored in pale green) bound to the RBD (gray surface, ACE2 binding site in yellow) of SARS-CoV spike ectodomain and for ADG-2 (cyan) bound to SARS-CoV-2 spike ectodomain. The homologous Fab ADI-19425 (PDB 6APC)

was docked in the ADG-2 cryo-EM map (EMD-23160) to generate the model. (**B**) DH1047 and ADG-2 bind partially overlapping binding sites on the RBD. (**C**) The therapeutic activity of DH1047, ADG-2, and control mAb in aged mice infected with SARS-CoV-2 B.1.351 was measured. Animals were treated at 6 hours post infection with the indicated antibodies and monitored for percent of starting weight (left) as well as lung viral replication titers (middle), and lung pathology (right) at 4 days post infection. Data are presented as mean±SEM (weight) or as mean (lung viral titer and lung pathology). Change in weight was compared using a two-way ANOVA followed by Tukey's multiple comparisons test, and differences in lung viral load and pathology were evaluated using a one-way ANOVA followed by Dunnett's multiple comparisons test. Differences in survival were measured by a Mantel-Cox test. *$p<0.05$; **$p<0.01$; ***$p<0.001$.

Table S1. Monoclonal antibody neutralization screen against SARS-CoV-2 2AA MA, SARS-CoV, WIV-1, and RsSHC014

Table S2. Cryo-EM data collection and refinements statistics.

Table S3. Immunogenetic characteristics of broadly cross-reactive mAbs.

Figure S1

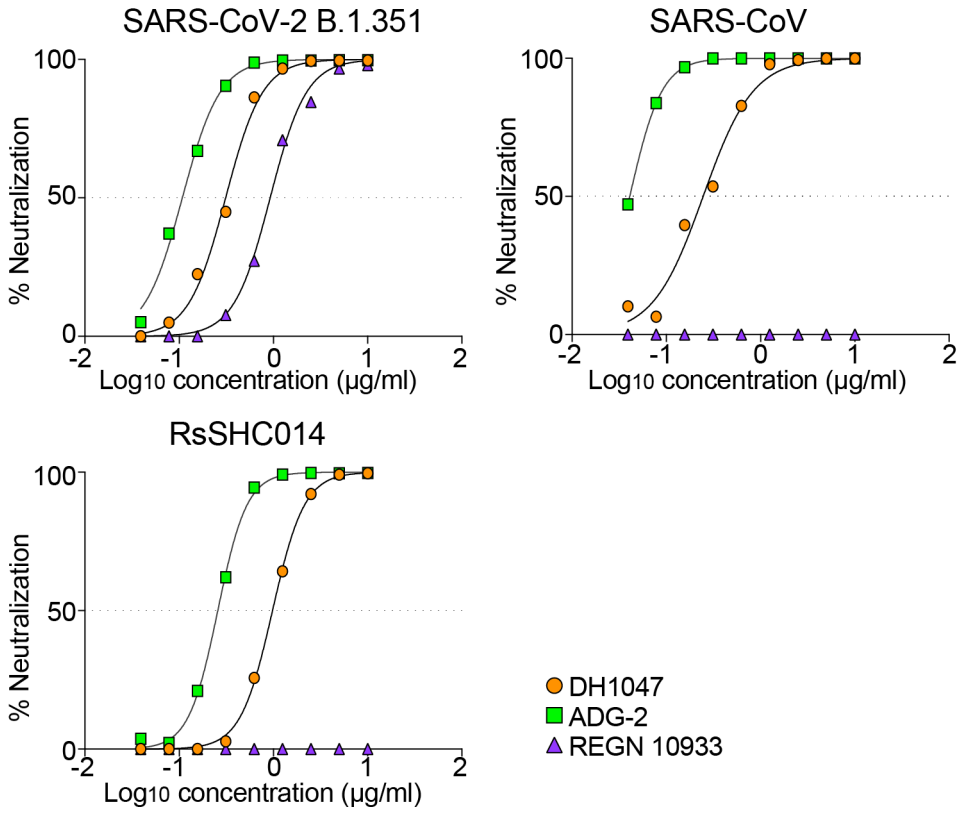
SARS-CoV-2 B.1.351
SARS-CoV
RsSHC014
% Neutralization
100
50
0
-2
-1
0
1
2
Log10 concentration (µg/ml)
DH1047
ADG-2
REGN 10933

Figure S2

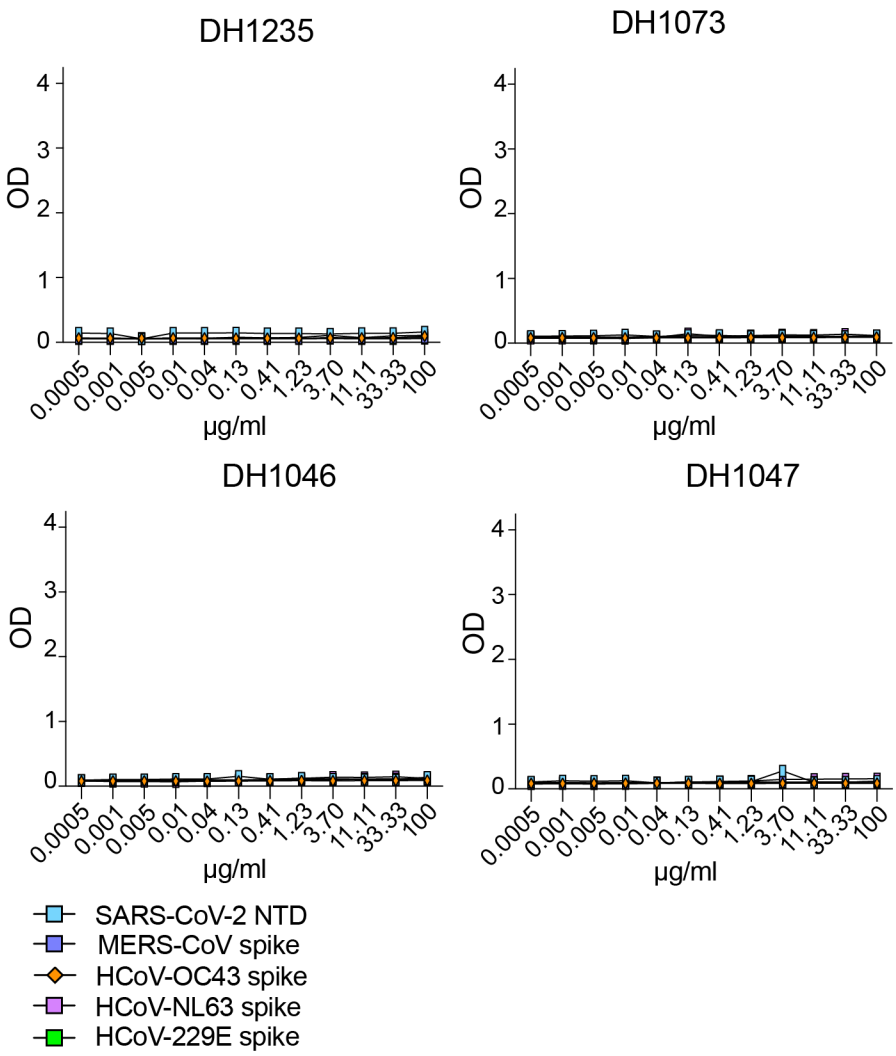
DH1235
DH1073
DH1046
DH1047
OD
µg/ml
0.0005
0.001
0.005
0.01
0.04
0.13
0.41
1.23
3.70
11.11
33.33
100
SARS-CoV-2 NTD
MERS-CoV spike
HCoV-OC43 spike
HCoV-NL63 spike
HCoV-229E spike

Figure S3

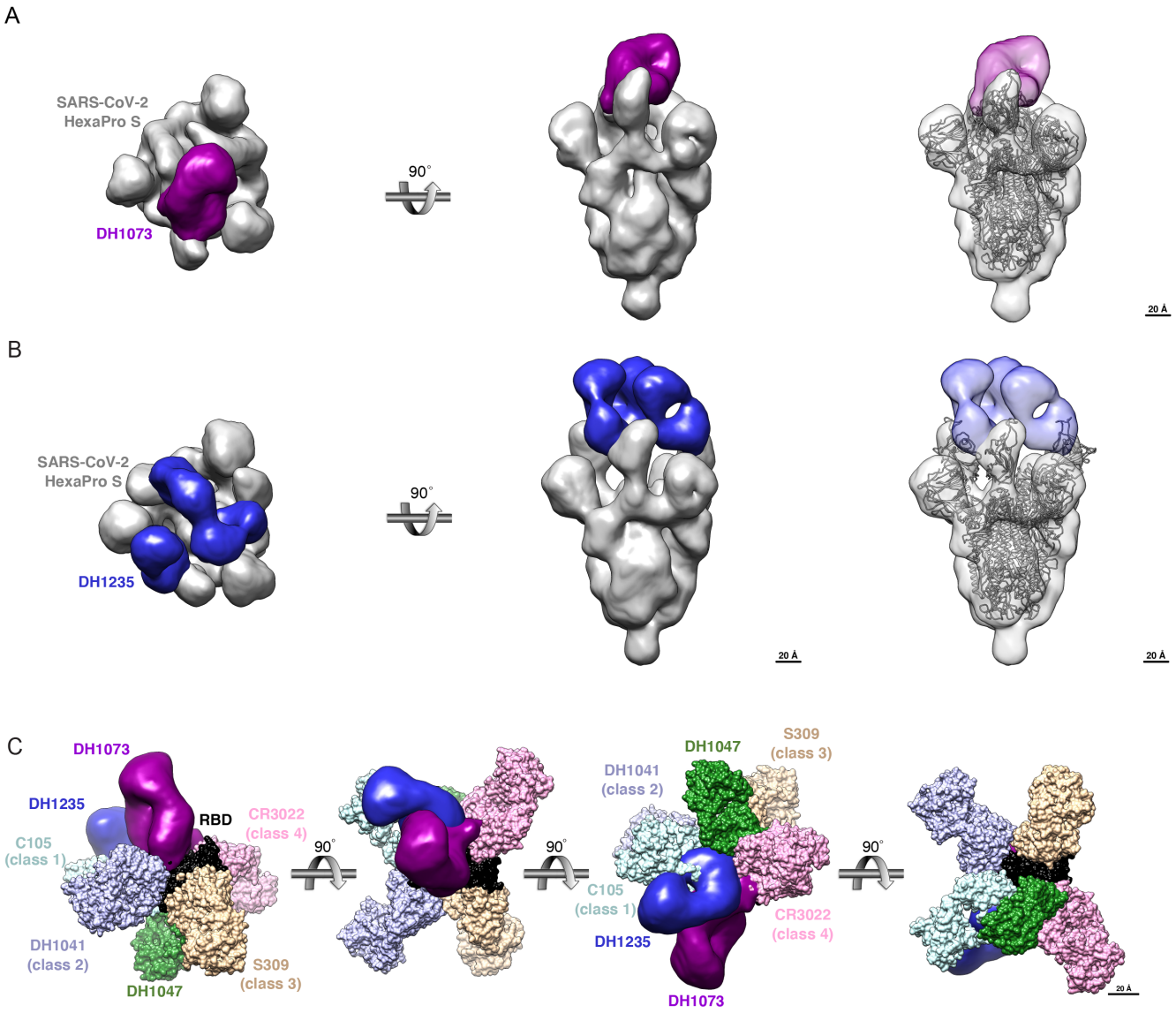

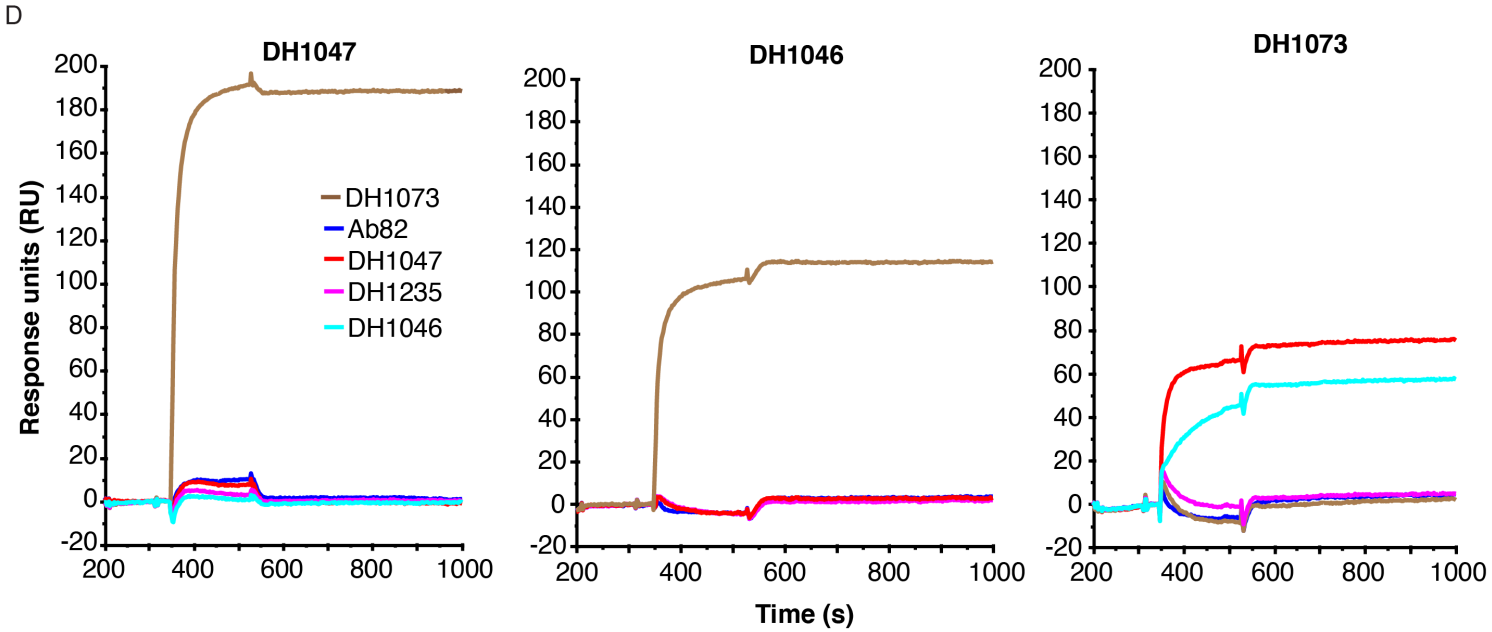

mAb	DH1046	DH1047	DH1073	DH1235
DH1046	+	+	-	+
DH1047	+	+	-	+
DH1073	-	-	+	+

- no competition

+ no competition

Figure S4

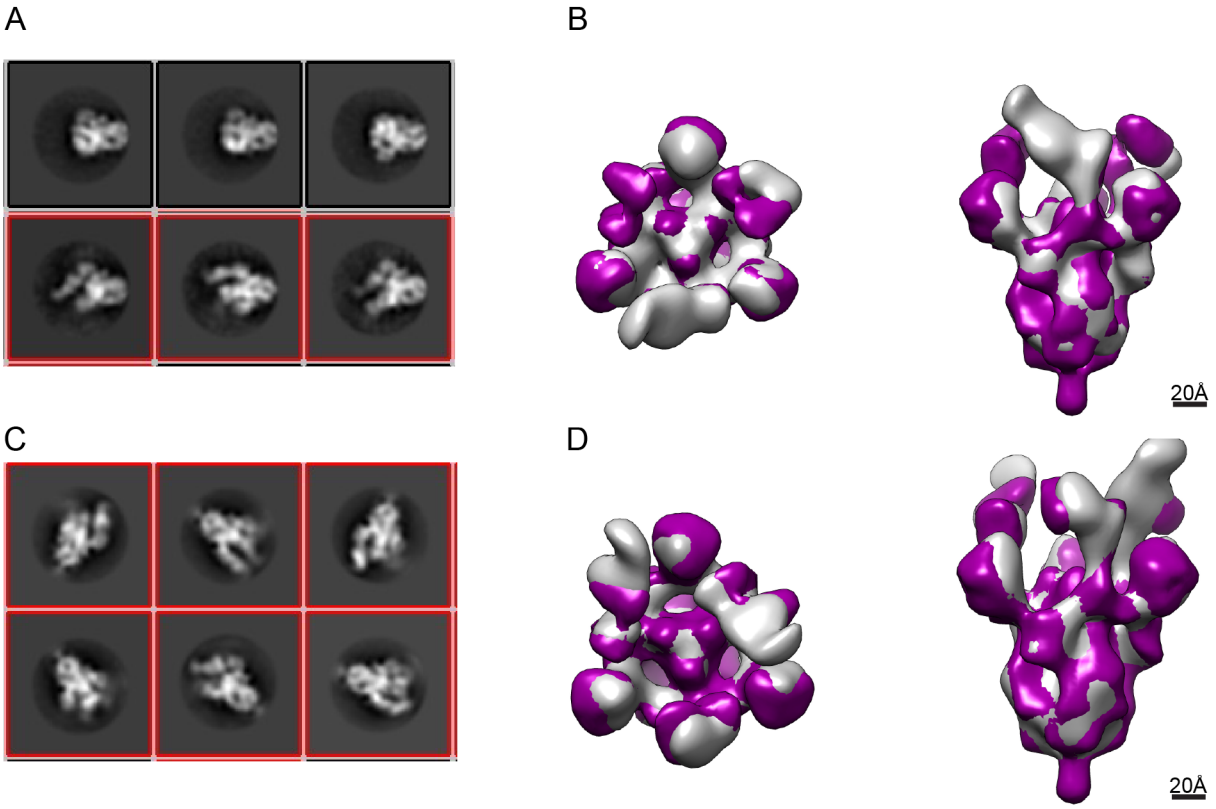

Figure S5

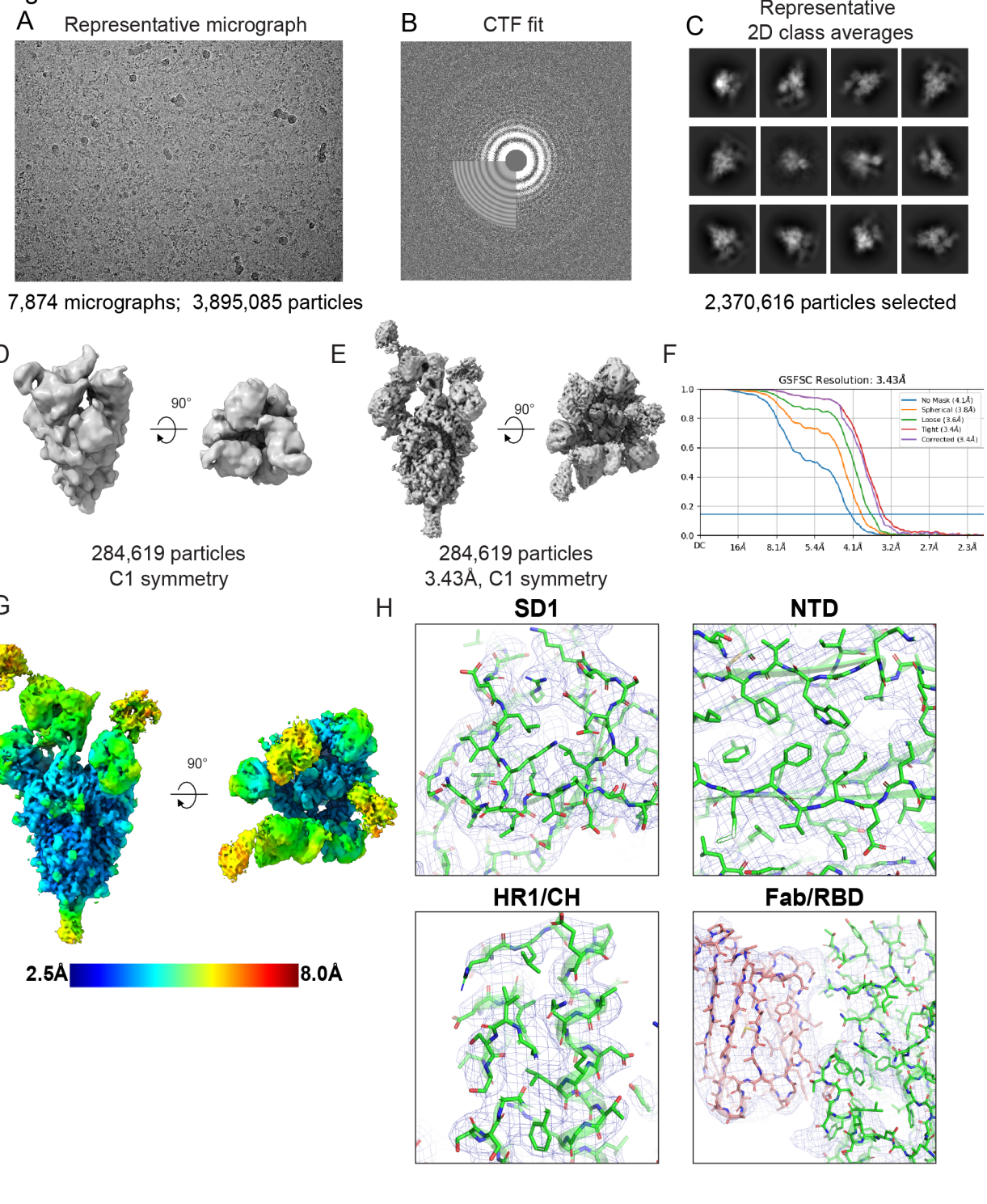
A
Representative micrograph
B
CTF fit
C
Representative
2D class averages
7,874 micrographs; 3,895,085 particles
2,370,616 particles selected
D
90°
284,619 particles
C1 symmetry
E
90°
284,619 particles
3.43Å, C1 symmetry
F
GSFSC Resolution: 3.43Å
No Mask (4.1Å)
Spherical (3.8Å)
Loose (3.6Å)
Tight (3.4Å)
Corrected (3.4Å)
1.0
0.8
0.6
0.4
0.2
0.0
DC
16Å
8.1Å
5.4Å
4.1Å
3.2Å
2.7Å
2.3Å
G
90°
2.5Å
8.0Å
H
SD1
NTD
HR1/CH
Fab/RBD

Figure S6

SARS-CoV Toronto spike			
Fab	ka (1/Ms)	kd (1/s)	KD(nM)
DH1047	9.622E+4	<1.0E-5	<0.1

RsSCH014 spike			
Fab	ka (1/Ms)	kd (1/s)	KD(nM)
DH1047	8.602E+4	<1.0E-5	<0.1

DH1047 Fab vs. SARS-CoV Toronto

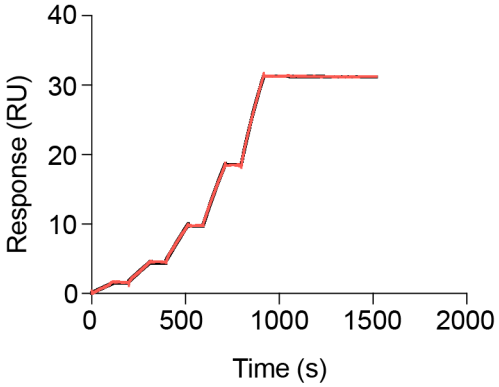

DH1047 Fab vs. RsSHc014

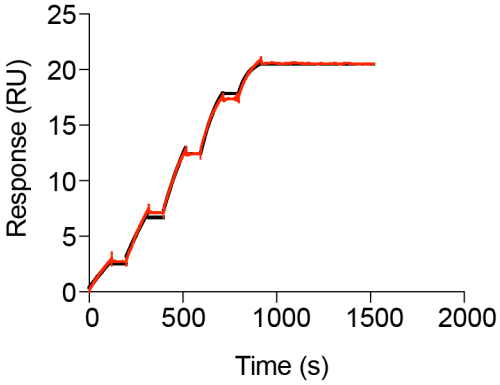

Figure S7

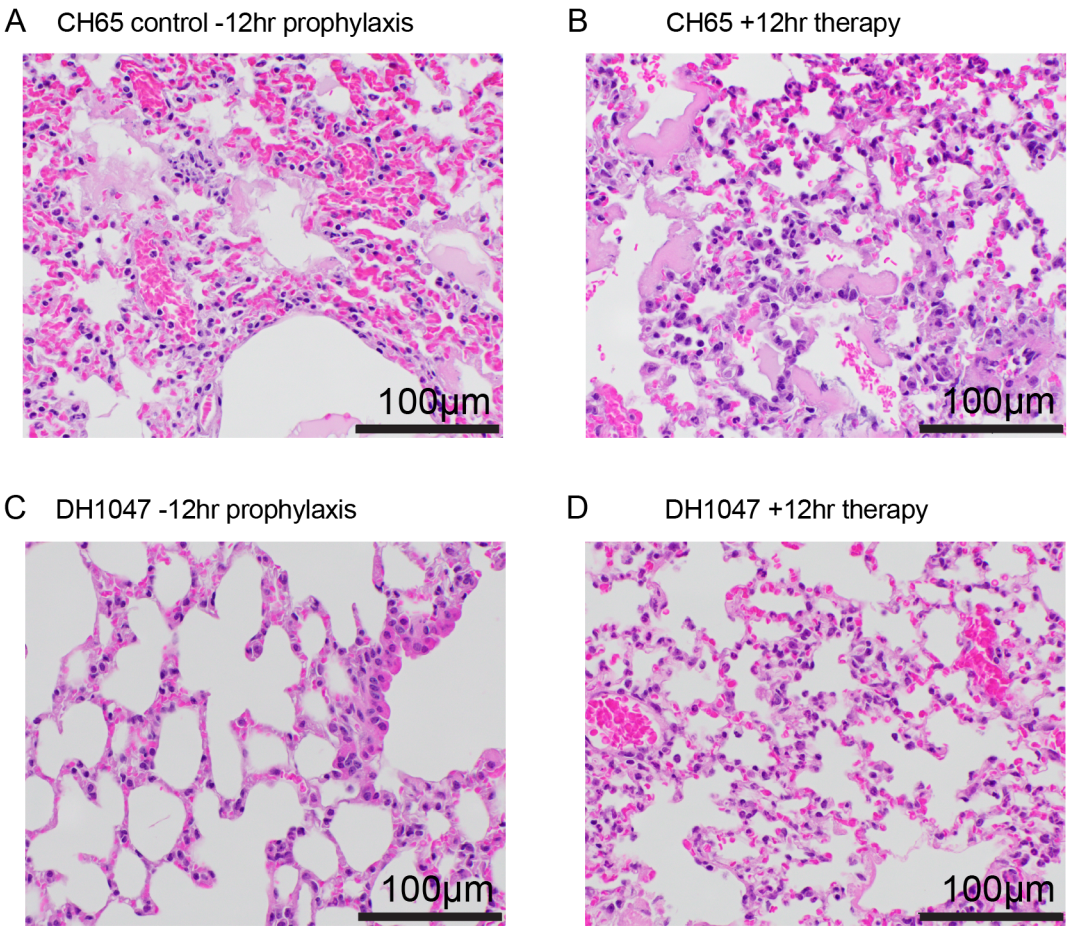
A
CH65 control -12hr prophylaxis
100µm
B
CH65 +12hr therapy
100µm
C
DH1047 -12hr prophylaxis
100µm
D
DH1047 +12hr therapy
100µm

Figure S8

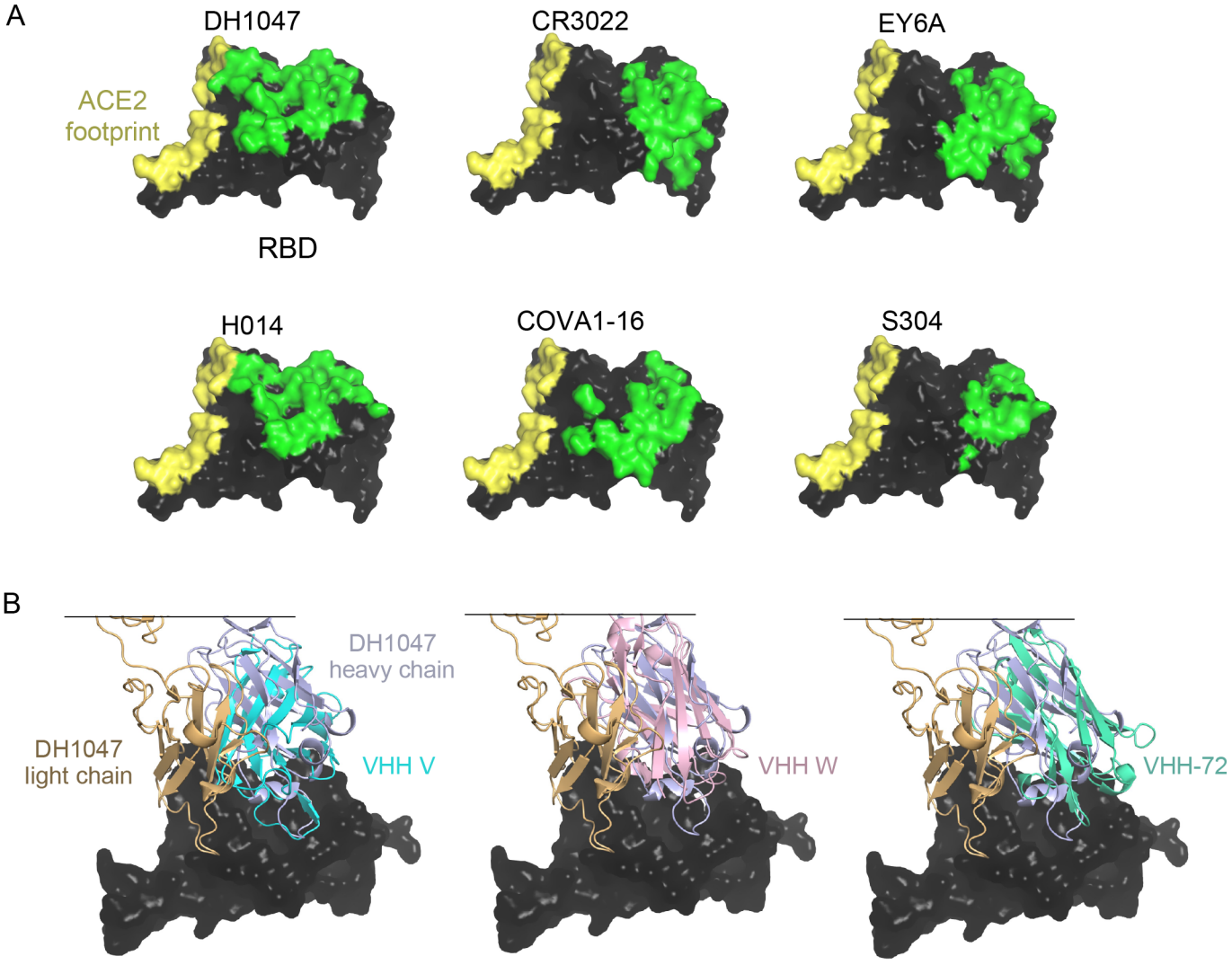
A
DH1047
CR3022
EY6A
ACE2
footprint
RBD
H014
COVA1-16
S304
B
DH1047
heavy chain
DH1047
light chain
VHH V
VHH W
VHH-72

Figure S9

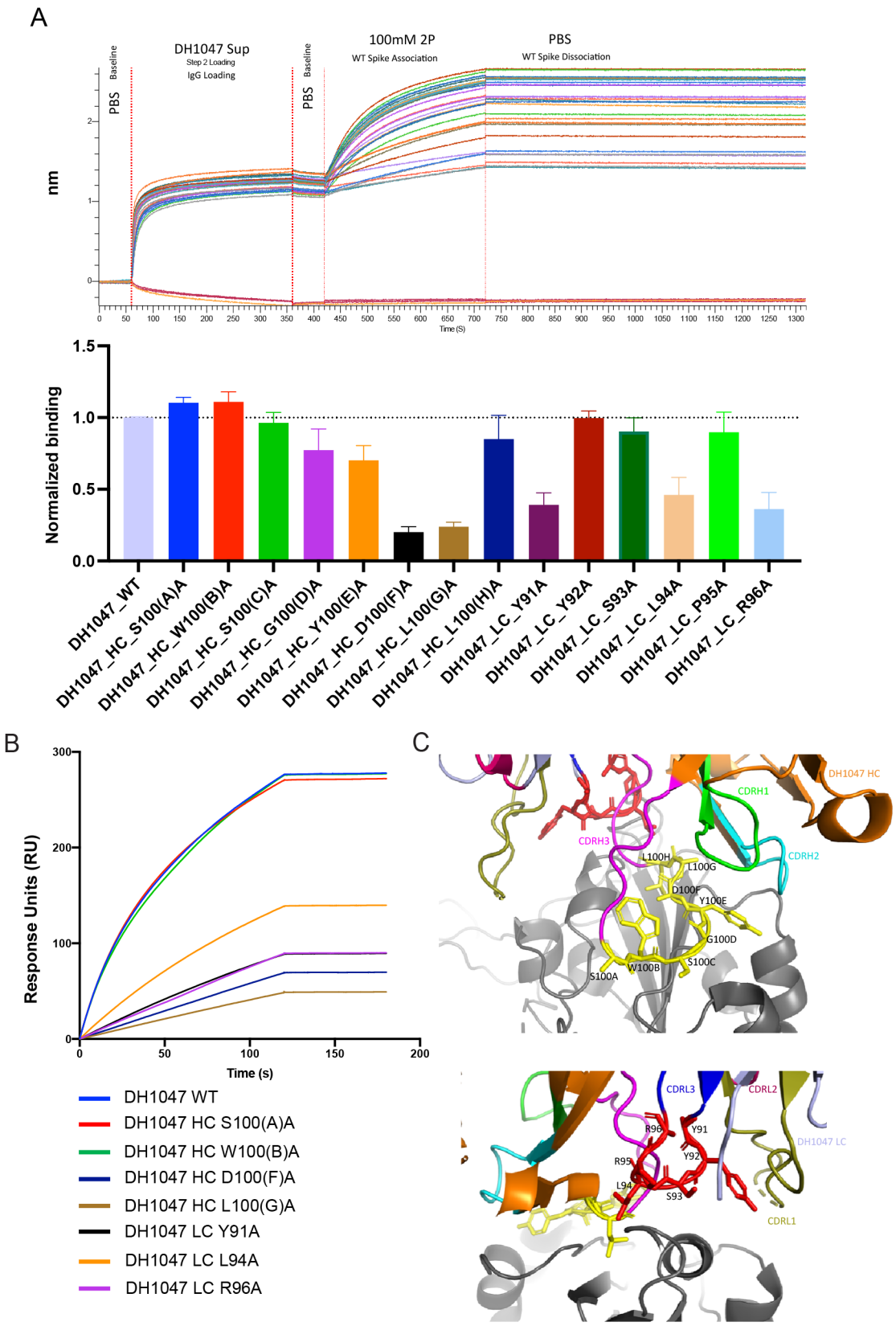
A
DH1047 Sup
Step 2 Loading
IgG Loading
100mM 2P
WT Spike Association
PBS
WT Spike Dissociation
Baseline
PBS
Baseline
PBS
nm
Time (S)
Normalized binding
DH1047_WT
DH1047_HC_S100(A)A
DH1047_HC_W100(B)A
DH1047_HC_S100(C)A
DH1047_HC_G100(D)A
DH1047_HC_Y100(E)A
DH1047_HC_D100(F)A
DH1047_HC_L100(G)A
DH1047_HC_L100(H)A
DH1047_LC_Y91A
DH1047_LC_Y92A
DH1047_LC_S93A
DH1047_LC_L94A
DH1047_LC_P95A
DH1047_LC_R96A
B
Response Units (RU)
Time (s)
DH1047 WT
DH1047 HC S100(A)A
DH1047 HC W100(B)A
DH1047 HC D100(F)A
DH1047 HC L100(G)A
DH1047 LC Y91A
DH1047 LC L94A
DH1047 LC R96A
C
DH1047 HC
CDRH1
CDRH3
CDRH2
L100H
L100G
D100F
Y100E
G100D
S100C
W100B
S100A
CDRL3
CDRL2
R96
Y91
Y92
R95
L94
S93
DH1047 LC
CDRL1

Figure S10

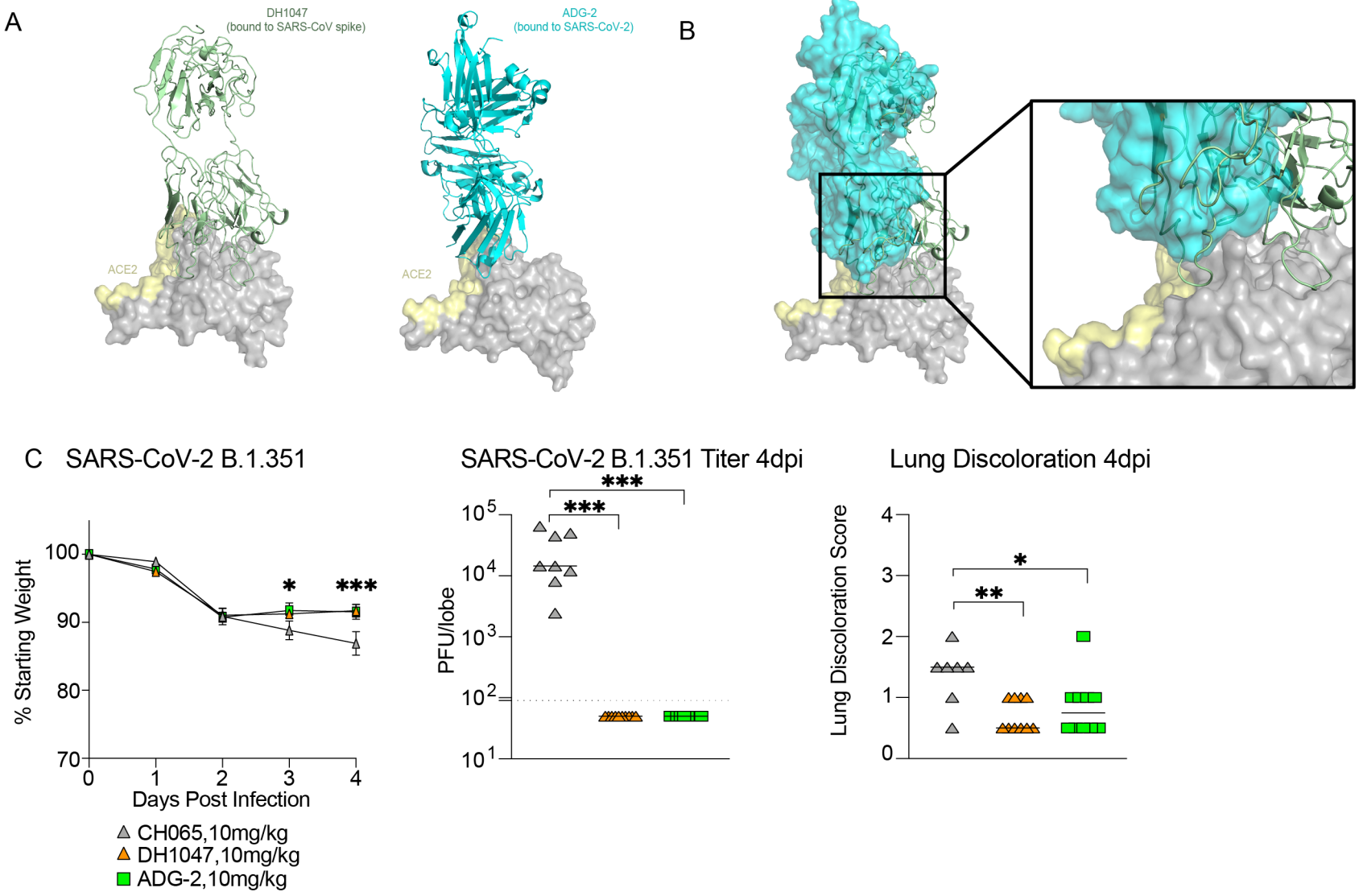
A
DH1047
(bound to SARS-CoV spike)
ACE2
ADG-2
(bound to SARS-CoV-2)
ACE2
B
C SARS-CoV-2 B.1.351
% Starting Weight
100
90
80
70
0
1
2
3
4
Days Post Infection
*
***
CH065,10mg/kg
DH1047,10mg/kg
ADG-2,10mg/kg
SARS-CoV-2 B.1.351 Titer 4dpi
PFU/lobe
10^5
10^4
10^3
10^2
10^1
***
***
Lung Discoloration 4dpi
Lung Discoloration Score
4
3
2
1
0
*
**

Table S1. Monoclonal antibody screen against SARS-CoV-2 2AA MA, SARS-CoV, WIV-1, and RsSHC014

mAb #	DH #	Specificity to SARS-CoV-2	ELISA cross-reactivity	Live virus neutralization IC_{50} (μg/ml)			
				SARS-CoV-2 2AA MA	SARS-CoV	WIV-1	RsSHC014
1	DH1058	S2	SARS-CoV-1, MERS-CoV, 229E, NL63, HKU1, OC43	>10	>10	>10	>10
2	DH1057	S2	SARS-CoV-1, OC43	>10	>10	>10	>10
3	**DH1047**	**RBD**	**SARS-CoV, SARS-CoV-2, and bat CoVs**	**0.3979**	**0.0287**	**0.191**	**0.2005**
4	DH1203	RBD	SARS-CoV and SARS-CoV-2	3.768	0.04781	>10	>10
5	DH1127	RBD	SARS-CoV and SARS-CoV-2	>10	>10	>10	>10
6	DH1059	no binding	SARS-CoV-2	>10	>10	>10	>10
7	DH1081	NTD	SARS-CoV and SARS-CoV-2	>10	>10	>10	>10
8	DH1085	no binding	SARS-CoV-2	>10	>10	>10	>10
9	DH1080	RBD	SARS-CoV and SARS-CoV-2	>10	0.0059	0.0330	>10
10	DH1061.1	NTD	SARS-CoV and SARS-CoV-2	>10	>10	>10	>10
11	DH1065	NTD	SARS-CoV and SARS-CoV-2	>10	>10	>10	>10
12	DH1066	NTD	only SARS-CoV	>10	>10	>10	>10
13	DH1064	RBD	SARS-CoV and SARS-CoV-2	>10	0.0216	>10	>10
14	DH1067	NTD	SARS-CoV and SARS-CoV-2	>10	>10	>10	>10
15	DH1069	NTD	SARS-CoV and SARS-CoV-2	>10	>10	>10	>10
16	**DH1046**	**RBD**	**SARS-CoV, SARS-CoV-2, and bat CoVs**	**2.857**	**0.1033**	**0.4248**	**1.274**
17	DH1068	NTD	SARS-CoV and SARS-CoV-2	>10	>10	>10	>10
18	DH1086	NTD	SARS-CoV and SARS-CoV-2	>10	>10	>10	>10
19	DH1071	NTD	SARS-CoV and SARS-CoV-2	>10	>10	>10	>10
20	DH1088	no binding	SARS-CoV-2	>10	>10	>10	>10
21	**DH1073**	**RBD**	**SARS-CoV, SARS-CoV-2, and bat CoVs**	**0.8088**	**0.0161**	**0.267**	**>10**
22	**DH1235**	**RBD**	**SARS-CoV, SARS-CoV-2, and bat CoVs**	**0.1226**	**0.0403**	**0.0602**	**>10**
23	DH1306	RBD	SARS-CoV and SARS-CoV-2	>10	>10	>10	>10
24	DH1193	RBD	SARS-CoV and SARS-CoV-2	4.345	>10	>10	>10
25	DH1152	RBD	SARS-CoV and SARS-CoV-2	>10	>10	>10	>10
26	DH1171	NTD	SARS-CoV and SARS-CoV-2	>10	>10	>10	>10
27	DH1109	RBD	SARS-CoV and SARS-CoV-2	>10	>10	>10	>10
28	DH1208	RBD	SARS-CoV and SARS-CoV-2	>10	>10	>10	>10
29	DH1166	RBD	SARS-CoV and SARS-CoV-2	>10	>10	>10	>10
30	DH1191	RBD	SARS-CoV and SARS-CoV-2	>10	>10	>10	>10
31	DH1120	RBD	SARS-CoV and SARS-CoV-2	>10	>10	>10	>10
32	DH1110	NTD	SARS-CoV and SARS-CoV-2	>10	>10	>10	>10
33	DH1106	NTD	SARS-CoV and SARS-CoV-2	>10	>10	>10	>10
34	DH1112	RBD	SARS-CoV and SARS-CoV-2	>10	0.0023	0.1617	>10
35	DH1117	RBD	SARS-CoV and SARS-CoV-2	>10	>10	>10	>10
36	DH1115	RBD	SARS-CoV and SARS-CoV-2	>10	0.0083	0.1614	>10
37	DH1093	NTD	SARS-CoV and SARS-CoV-2	>10	>10	>10	>10
38	DH1095	RBD	SARS-CoV	>10	>10	>10	>10
39	DH1113	RBD	SARS-CoV and SARS-CoV-2	>10	>10	>10	>10
40	DH1114	NTD	SARS-CoV and SARS-CoV-2	>10	>10	>10	>10
41	DH1098	RBD	SARS-CoV and SARS-CoV-2	>10	0.0052	0.0318	>10
42	DH1101	RBD	SARS-CoV and SARS-CoV-2	>10	0.0012	>10	>10
43	DH1298	RBD	SARS-CoV and SARS-CoV-2	>10	0.0399	0.4312	>10
44	DH1299	RBD	SARS-CoV and SARS-CoV-2	>10	>10	>10	>10
45	DH1300	RBD	SARS-CoV and SARS-CoV-2	>10	>10	>10	>10
46	DH1301	RBD	SARS-CoV and SARS-CoV-2	>10	>10	>10	>10
47	DH1302	RBD	SARS-CoV and SARS-CoV-2	>10	>10	>10	>10
48	DH1303	RBD	SARS-CoV and SARS-CoV-2	>10	>10	>10	>10
49	DH1304	RBD	SARS-CoV and SARS-CoV-2	>10	>10	>10	>10
50	DH1305	RBD	SARS-CoV and SARS-CoV-2	9.877	>10	>10	>10

PDB ID 7SG4 EMDB ID EMD-25105	
Data collection and processing	
Microscope	FEI Titan Krios
Detector	Gatan K3
Magnification	81,000
Voltage (kV)	300
Electron exposure (e–/Å2)	54.1
Defocus range (μm)	~0.75-2.50
Pixel size (Å)	1.08
Reconstruction software	cryoSparc
Symmetry imposed	C1
Initial particle images (no.)	2,370,616
Final particle images (no.)	284,619
Map resolution (Å)	3.43
FSC threshold	0.143
Refinement	
Initial model used	7LD1
Model resolution (Å)	3.43
FSC threshold	0.143
Model composition	
Nonhydrogen atoms	28,712
Protein residues	3,737
R.m.s. deviations	
Bond lengths (Å)	0.013
Bond angles (°)	1.906
Validation	
MolProbity score	1.C9
Clashscore	0.2
Poor rotamers (%)	2.01
EM ringer score	2.83
Ramachandran plot	
Favored (%)	88.89
Allowed (%)	9.53
Disallowed (%)	1.58

Table S3. Immunogenetic characteristics of broadly cross-reactive mAbs

DH#	Antibody ID	Binding Specificity	Cross Reactivity	Antibody Gene Analysis									
				Donor ID	Time Point	HCDR3 Length	Heavy chain mutation	VH_Gene	JH_Gene	LCDR3 Length	Light chain mutation	VL_Gene	JL_Gene
DH1235	Ab026319_LS	RBD	SARS-CoV-1	SARS-CoV-2 convalescent	Day 36	21	1.68	IGHV3-48	IGHJ4	9	1.75	IGLV4-60	IGLJ2
DH1073	Ab026258_LS	RBD	SARS-CoV-1	SARS-CoV convalescent	Year 17	15	9.06	IGHV1-46	IGHJ6	11	2.92	IGKV3-11	IGKJ1
DH1046	Ab026204_LS	RBD	SARS-CoV, PCoV GXP4L, Bat CoV RsSHC014, Bat CoV RaTG13	SARS-CoV convalescent	Year 17	24	4.70	IGHV3-23	IGHJ6	9	3.65	IGKV1-5	IGKJ2
DH1047	Ab712384_LS	RBD	SARS-CoV, PCoV GXP4L, Bat CoV RsSHC014, Bat CoV RaTG13	SARS-CoV convalescent	Year 17	24	8.05	IGHV1-46	IGHJ4	9	2.05	IGKV4-1	IGKJ1